Applied Catalysis B: Environmental 209 (2017) 12–22

Contents lists available at ScienceDirect

Applied Catalysis B: Environmental

journal homepage: www.elsevier.com/locate/apcatb

Probing the synergistic ratio of the NiMo/γ-Al_2O_3 reduced catalysts for the transformation of natural triglycerides into green diesel

Eleana Kordouli[a], Labrini Sygellou[b], Christos Kordulis[a,b], Kyriakos Bourikas[c,*], Alexis Lycourghiotis[a]

[a] Department of Chemistry, University of Patras, GR-26504 Patras, Greece
[b] Foundation for Research and Technology, Institute of Chemical Engineering Science (FORTH/ICE-HT), Stadiou Str., Platani, P.O. Box 1414, GR-26500 Patras, Greece
[c] School of Science and Technology, Hellenic Open University, Tsamadou 13-15, GR-26222, Patras, Greece

ARTICLE INFO

Article history:
Received 25 October 2016
Received in revised form 10 February 2017
Accepted 11 February 2017
Available online 14 February 2017

Keywords:
NiMo/γ-Al_2O_3 reduced catalysts
Biofuels
Renewable diesel
Selective deoxygenation
Synergistic ratio

ABSTRACT

The synergistic atomic ratio, $\frac{Ni}{Ni+Mo}$, of the NiMo/γ-Al_2O_3 *reduced* catalysts was investigated for the transformation of natural triglycerides into green diesel. A series of catalysts with different atomic ratios $0 \leq \frac{Ni}{Ni+Mo} \leq 1$ and constant atomic surface density (Mo + Ni) = 4 atoms/nm^2 was prepared and characterized using adsorption–desorption isotherms, XRD, SEM-EDS, XPS and H_2-TPR. The catalysts were evaluated in the selective deoxygenation of sunflower oil performed by hydrotreatment using a semi-batch reactor. For comparison, two additional NiMo/γ-Al_2O_3 *sulphided* catalysts were synthesized and tested. The most active *reduced* catalyst was also tested in the selective deoxygenation of waste cooking oil.

MoO_3/MoO_x (Mo oxidation number between 5 and 4) and Ni^0, NiO, $NiAl_2O_4$ phases very well dispersed on the support surface and uniformly distributed on the catalysts extrudates have been detected in all cases. The high dispersion of these phases does not practically disturb the texture of the support which exhibits a single peak pore volume distribution centered at about 8–9 nm. The Ni, Mo composition of the catalysts somehow affects the relative amounts of these phases of the same element.

It was found that the aforementioned $\frac{Ni}{Ni+Mo}$ ratio is located at about 0.8. This is very different to that of the *sulphided* catalysts which is located at about 0.3 for both the hydrodesulphurization of petroleum fractions and the selective deoxygenation of sunflower oil. An impressive increase of the% yield to hydrocarbons in the diesel range by a factor of 4.77 was achieved by a simple change of the $\frac{Ni}{Ni+Mo}$ atomic ratio in the NiMo/γ-Al_2O_3 *reduced* catalysts from 0.3 to 0.8. A complete transformation of both sunflower oil and waste cooking oil into hydrocarbons in the diesel range was obtained over the most active catalyst at 310 °C, hydrogen pressure 40 bar, reactant volume to catalyst mass ratio equal to 10 ml/g and reaction time equal to 5 h.

1. Introduction

Humanity is facing a climate change due to the emission of carbon dioxide from the combustion of fossil fuels. This is mainly responsible for the global warming. On the other hand the amount of the fossil fuels is not unlimited. It is well established that the increasing demands for fossil fuels are expected to lead to the progressive depletion of oil reserves during the 21st century [1]. The gradual replacement of fossil fuels by renewable energy is imperative for overcoming both problems [1–3]. Biomass is an important source of renewable energy. Using microalgal oils as a source of natural triglycerides [4] or industrializing natural photosynthesis using genetically modified Cyanobacteria [2] are welcomed future prospective for producing biofuels, facing the competition between foods and renewable energy and capturing carbon dioxide. The use of waste cooked oils is also another environmentally benign alternative. However, for the present time we are enforced using mainly biomass drawn from energy plants. The natural triglyceride based biomass (vegetable oils, animal fat and cooked oils) is currently used for producing biodiesel, one of the two most important bio-fuels [5]. The biodiesel, a mixture of fatty acid methyl esters, is produced by transesterification of natural triglycerides,

* Corresponding author.
E-mail address: bourikas@eap.gr (K. Bourikas).

http://dx.doi.org/10.1016/j.apcatb.2017.02.045
0926-3373/

mainly with methanol [5]. The very simple technology and the mild reaction conditions allow the biodiesel production in small units practically installed everywhere. However, the chemical composition of biodiesel (mixture of esters) is implicated for several problems concerning its storage whereas it limits its use as car fuel in "bio-diesel/oil-diesel" mixtures with relatively low ratio. Another problem is related with the accumulation of large amounts of low quality glycerol, considered as an unwanted waste [6].

The above problems have stimulated intensive research for developing alternative processes for triglycerides upgrading resulting to the production of hydrocarbons instead of fatty acid methyl esters [4,7,8]. The cracking/hydrocraking of natural triglycerides seems to be a promising process [9,10]. This can be performed at relatively high reaction temperature (400–550 °C) and atmospheric pressure over acidic microporous and mesoporous catalysts. The main advantage of the process is that it is realized in the absence or in the presence of small amount of hydrogen. However, this upgrading approach presents two weaknesses. The *organic liquid product* produced is a mixture of hydrocarbons in the range of gasoline, kerosene and diesel. Therefore, a subsequent separation step is needed for obtaining useful bio-fuels. Moreover, the acidic catalysts used are easily deactivated due to the coke formation.

By hydrotreating natural triglycerides in lower temperatures (260–360 °C) and high hydrogen pressures (10–80 bar) over catalysts with mild acidity the so called *selective deoxygenation* (SDO) can be achieved [4,7,11]. This is realized by *decarboxylation,* deCO$_2$, where oxygen is removed in the form of CO$_2$, *decarbonylation*, deCO, where oxygen is removed in the form of water and CO and/or *hydrodeoxygenation*, HDO, where oxygen is removed in the form of water. In all cases the fragmentation of side chains of triglycerides kept low and thus alkanes in the diesel range (C15–C18) are usually obtained (*green diesel*). This renders SDO a quite promising upgrading process.

Two types of catalysts were initially investigated for SDO in the frame of the so called *stand alone* industrial approach where the triglycerides are treated separately from the petroleum fractions, the noble metals and the conventional Co(Ni)Mo(W)/γ-Al$_2$O$_3$ sulphided hydrodesulphurization (HDS) catalysts [4,7,11]. Supported noble metals are very active and selective, mainly palladium. Nevertheless, their high cost and limited availability render this kind of catalysts rather not viable for industrial use. The sulphided catalysts are also very effective. The problem here is that we have to maintain the catalyst in their sulphided form by passing a compound containing sulphur in the reactor. This can cause unwanted S-contamination of the produced green diesel [12]. The above have redirected research into *nickel based non-sulphided catalysts* which are also less expensive than the noble metal ones. Ni catalysts of various forms (mono-elemental and bi-elemental reduced, phosphides, carbides and nitrides) supported on various carriers and prepared by different methods have been characterized and tested using various feedstock. The subject has been very recently reviewed by us [13].

Comparison of the conventional Co(Ni)Mo(W)/γ-Al$_2$O$_3$ sulphided HDS catalysts with their counterparts in the reduced form (non-sulphided) has shown that the sulphided catalysts are considerably more active than the corresponding reduced ones [14–16]. In order to confront this problem an effort has been recently undertaken to develop Co(Ni)-Mo(W)/γ-Al$_2$O$_3$ reduced catalysts with higher activities, similar to those of the corresponding sulphided ones [14–19]. This was obtained by doping the support with lanthana [14,15], ceria [5] or phosphorous [17–19]. In fact, the resulting reduced catalysts have shown similar catalytic activity to the corresponding, non doped, sulphided ones [17–19]. In most of these studies the catalysts had a promoter (Co, Ni) to active element (Mo, W) ratio equal or very similar to that of the conventional Co(Ni)Mo(W)/γ-Al$_2$O$_3$ sulphided catalysts used in HDS of petroleum fractions, namely the synergistic ratio $\frac{Ni}{Ni+Mo} = 0.3$ [20]. This implied the underlined assumption that this critical ratio is the same for both types of catalysts (sulfided, reduced) and processes (HDS, SDO).

The main goal of this work is to investigate the aforementioned assumption probing the synergistic $\frac{Ni}{Ni+Mo}$ atomic ratio of the NiMo/γ-Al$_2$O$_3$ reduced catalysts for the transformation of natural triglycerides into green diesel. To do that we have prepared a series of NiMo/γ-alumina reduced catalysts (extrudates) with constant total atoms surface density (Ni + Mo = 4 atoms/nm^2) attaining monolayer coverage of the support surface and various Ni/Mo atom ratios. The catalysts were characterized, using adsorption–desorption isotherms, XRD, SEM-EDS, XPS and H$_2$-TPR and evaluated in the SDO of sunflower oil (SO) using a semi-batch reactor. For comparison two additional NiMo/γ-alumina sulphided catalysts were synthesized and tested. The most active reduced catalyst was also tested in the SDO of waste cooking oil (WCO). To the extent of our good knowledge it is not yet a study dealing with the SDO of SO and WCO over nickel based non-sulphided catalysts [13]. The comparison of the reactivity of these different feedstocks with respect to SDO is also another purpose of the present work.

1.1. Considerations on H_2 and feedstocks

There is no doubt that hydrogen is a valuable molecule for many hydrotreatment applications, including the prospect of carbon dioxide recyclization. For the moment, it is mainly produced from the steam reforming of natural gas and petrol oils and only a very few portion from water electrolysis. This situation is expected to be changed drastically due to the drastic development of the renewable sources of energy, mainly those of photovoltaic and wind farms. One way for energy storage is the use of the excess electricity produced from renewable sources for hydrogen production through water electrolysis [21].

The SO is largely used in several countries, among which Greece, as a raw material for producing biodiesel. This means that the process based on SO is economically feasible taking into account the politics for promoting renewable energy. Thus, one may expect that SO would be used in the near future for producing green diesel. Relevant studies have shown that the production of green diesel is economically favourable or of equal cost compared to the production of biodiesel [22–24]. Concerning the amount of available SO, it should be mentioned that this is not sufficient to replace the whole amount of the petro-diesel now day used. This is also true for all vegetable, algal, and waste coked oils. However, the prospect for the partial replacement of petro-diesel by renewable diesel is quite probable own to the environmental demands and the evolution of agricultural technology. For instance, although SO is a typical edible oil crop, genetically modified sunflower grown on marginal land such as old mining lands and irrigation canals has been identified as one of the sustainable biofuel sources since it does not encroach upon arable lands [25]. These sunflower plants require low moisture and fertility demands allowing them to grow on marginal land. The sunflower seeds contain a high oil content (about 50%), but the oil quality does not meet food standards [25].

The WCO is also used in our country to produce biodiesel. Due to the large number of touristic enterprises the collection of relatively large amounts of WCO, imposed by the environmental legislation, provides, in effect, a very cheap and actually renewable raw material for producing green diesel. Large quantities of waste cooking oils (~100 million gallons/d are produced in USA) and animal fats are available throughout the world, especially in the developed countries [26]. The quantities of waste cooking oils produced in Greece are calculated to be 300–400 thousand tones/yr corresponding to ~30% of diesel used in transportation sector. Management of

Table 1
Feedstocks characteristics.

Property	WCO	SO
Density at 25 °C/g ml^{-1}	0.894	0.892
Viscosity Kinematic[a]/cSt	9.89	7.93
Acidity (%)	0.83	0.04
Iodine number	115.0	128.7
Oligomers (wt%)	1.5	–

[a] Measured at 93.3 °C.

such oils and fats poses a significant challenge because of their disposal problems and possible contamination of the water and land resources. Even though some of this waste cooking oil is used for soap production, a major part of it is discharged into the environment [26].

2. Experimental

2.1. Feedstocks

The natural triglycerides of the SO have side chains corresponding to about eleven fatty acids in the range of 16–20 carbon atoms. Most side chains correspond to linoleic acid (18C atoms, two double bonds, 71.7%), oleic acid (18C atoms, one double bond, 15.9%), palmitic acid (16C atoms, saturated, 5.8%) and stearic acid (18C atoms, saturated, 3.9%).

The WCO used in this study, obtained by the "collectoil" company, was filtered three times using cloth filters of different sizes and then it was centrifuged prior to its use. Table 1 contains some crucial characteristics of the feedstocks used.

2.2. Preparation and activation of the catalysts

Gamma-alumina extrudates (AKZO, HDS-000-1,5mmE, SSA = 264 m^2/g, pore volume: 0.65 cm^3/g) were used as support. The Mo species were first mounted by incipient wetness impregnation of the carrier with an ammonium heptamolybdate aqueous solution ($(NH_4)_6Mo_7O_{24}{\cdot}4H_2O$, Alfa Aesar) followed by drying at 110 °C overnight and air-calcination at 300 °C for 3 h. The nickel species were then deposited by incipient wetness impregnation of the precursor solid with a nickel nitrate solution ($Ni(NO_3)_2$ $6H_2O$, Merck, kGaA) and the solid was again dried at 110 °C overnight. The sample (2 g) was activated by reduction in a fixed bed reactor working under atmospheric pressure. The initial increase of temperature up to 400 °C (10 °C/min) under argon atmosphere (20 ml/min) was followed by activation under hydrogen flow (20 ml/min) at this temperature for 2.5 h and then by a decrease of temperature up to room temperature, again under argon atmosphere (20 ml/min). Two of the samples were sulphided at 400 °C for 2.5 h using a mixture of H_2/H_2S (85/15 v/v). The activation of each sample was ended by its passivation feeding the reactor at room temperature with 1 v/v% O_2 in Ar stream (20 ml/min) for 0.5 h.

2.3. Characterization of the catalysts

2.3.1. Scanning Electron Microscopy measurements

The morphology and chemical composition of the activated catalysts (extrudates) were examined using a Scanning Electron Microscope (SEMJEOL JSM6300). This is equipped with an Energy Dispersive Spectrometer (EDS). The chemical composition of the catalysts was determined using natural and synthetic standards and 20 kV accelerating voltage with 10 nA beam current. Microanalysis was performed on an epoxy resin polished and gold coated cross section perpendicular to the long axis of the extrudates.

2.3.2. Determination of the BET specific surface area and the pore volume distribution

The specific surface area of the activated samples has been determined by elaborating nitrogen sorption isotherms recorded using a Micromeritics apparatus (Tristar 3000 porosimeter) and the corresponding software. The BJH method was adopted for determining the pore size distributions.

2.3.3. Temperature programmed reduction

The TPR experiments were performed in a laboratory-constructed equipment described elsewhere [27]. An amount of sample, 0.04 g, was placed in a quartz reactor and the reducing gas mixture (H_2/Ar: 5/95 v/v) was passed through it for 2 h with a flow rate of 40 ml min^{-1} at room temperature. Then the temperature was increased to 1000 °C with a constant rate of 10 °C min^{-1}. Reduction leads to a decrease of the hydrogen concentration of the gas mixture, which was detected by a thermal conductivity detector (TCD) (Shimadzu). The reducing gas mixture was dried in a cold trap (−95 °C) before reaching the TCD.

2.3.4. Determination of crystal phases and crystal sizes by XRD

X-ray diffraction patterns were used for determining the crystal phases which are formed after activation of powdered samples. The XRD patterns were recorded in a Bruker D8 Advance diffractometer equipped with a nickel-filtered CuKα (1.5418 Å) radiation source. The step size and the time per step were respectively fixed at 0.02° and 0.5 s in the range of $10^{\circ} \leq 2\theta \leq 80^{\circ}$. The mean size of nanocrystals was determined using the Scherrer equation.

2.3.5. X-ray photoelectron spectroscopy

The surface analysis was performed on the reduced powdered samples pressed into suitable holders. In order to overcome eventual oxidation of the samples upon exposure to atmospheric air, these were re-reduced in the preparation chamber of the XPS machine at 400 °C for 6 h. The analysis was performed in a UHV chamber ($P < 10^{-9}$ mbar) equipped with a SPECS LHS-10 hemispherical electron analyzer. The XPS measurements were carried out at room temperature using non-monochromatized AlKa radiation under conditions optimized for maximum signal (constant ΔE mode with pass energy of 97 eV giving a full width at half maximum (FWHM) of 1.7 eV for the Au 4f7/2 peak). The analyzed area was an ellipsoid with dimensions 2.5 × 4.5 mm^2. The XPS core level spectra were analyzed using a fitting routine, which allows the decomposition of each spectrum into individual mixed Gaussian-Lorentzian components after a Shirley background subtraction. Wide Scans were recorded for all samples, while the core level peaks that were recorded in detail were: Mo3d, Ni2p, Al2p, C1s and O1s. Errors in our quantitative data are found in the range of ∼10% (peak areas), while the accuracy for BEs assignments is ∼0.1 eV.

2.4. Evaluation of the catalysts

2.4.1. Catalytic tests

A falling basket batch reactor (300 ml, Autoclave Engineers) working in a semi-batch mode was used for evaluating the catalysts. 100 ml of SO or WCO was introduced in the reactor vessel. An amount (1 g) of activated catalyst (extrudates) was added to the reactor basket being maintained at its upper position. After that the reactor was purged three times with Ar prior to be pressurized with H_2 (40 bar). The hydrogen flow rate was controlled to 100 ml/min by a flow controller (Brooks 58505S) and the speed of stirring to 1000 rpm. The reactor was heated with a temperature rate 10 °C/min to the reaction temperature (310 °C). Then the basket was falling into the liquid phase. This was the starting point of the reaction. A liquid sample of 2 ml was withdrawn from the

reactor every hour and analyzed. The reaction was monitored for a period of 9 h.

2.4.2. Chromatographic and GC–MS analysis

The liquid samples were analyzed by gas chromatography using a Shimadzu GC-2010 plus gas chromatograph equipped with a flame ionization detector (FID) and an appropriate column (SUPELCO, MET-Biodiesel, l = 14m, d = 0.53 mm, tf = 0.16 μm). The increase of temperature in the oven of the chromatograph followed the protocol: 50 °C for 2 min, increase up to 180 °C with a rate of 11 °C/min, 180 °C for 2 min, increase up to 230 °C with a rate 7 °C/min, 230 °C for 1 min, increase up to 380 °C with a rate 15 °C/min, 380 °C for 2 min. The temperature in the injector (350 °C) and detector (390 °C) remained constant during analysis. The sample to be analyzed was diluted with heptane (sample to heptane ratio equal to 1:20) and 1 μl of the diluted sample was injected into the GC with a split ratio of 40. High injection and column temperatures were used to directly analyze triglyceride without chemical derivatization [28]. Standard n-alkanes (n-C7–n-C25, SUPELCO) were used for product identification and calibration. The product identification was confirmed with a gas chromatograph-mass spectrometer (Shimadzu GCMS-QP2010 Ultra). The external standard (heptane) method was adopted for determining the composition of the sample. Gas-phase analysis was performed on line for selected experiments. The gas composition was determined using a six-port sampling valve and a Shimadzu GC-8A chromatograph equipped with a thermal conductivity detector and an appropriate column (SUPELCO, 110/120 Carbosieve S II, 10F, 1/8 in).

The determination of the composition of the liquid samples drawn allowed determining the percentage oil conversion as well as the weight percentage yield to each product. More precisely the % oil conversion is defined as $[(m_0 - m)/m_0] \times 100$ (m_0: initial mass of oil, m: mass of oil at a given time) and it was determined chromatographically using the formula $[(S_0/S_h) - (S/S_h)/(S_0/S_h)] \times 100$ where S_0 and S stand, respectively, for the total peak area of the peaks corresponding to SO or WCO at zero time and a given time whereas S_h stands for the peak area of heptane used as external standard. The S value was corrected to take into account the masses of the gaseous products. A correction factor was used equal to the mean value of the correction factors mentioned below (0.91). The following procedure was adopted for determining the composition of the liquid phase during reaction concerning all final products and byproducts. Known quantities of produced molecules were dissolved in n-C10 and after dilution with n-C7 (1/20) were used for preparing the corresponding calibration curves {[(S/S_h) versus wt% of a product in the liquid], S and S_h stand, respectively, for the peak area of the given product and the heptane used as external standard}. Then the ratio (S/S_h) based on a sample taken from the reactor was determined and the wt% composition in the given product was calculated by interpolation in the calibration curve. In order to transform the values of the wt% composition for each product (or by product) into the corresponding yield values we multiplied the above wt% values by the suitable normalization factors (HC: 0.80, FFA: 0.95, Big esters: 0.88, diglycerides: 1.0, small esters: 1.0). These factors have been calculated considering the transformation of tristearin molecule into each one of the aforementioned liquid products taking into account the mass loss of the initial oil due to the production of gases (Propane, ethane, methane, water, carbon monoxide and carbon dioxide).

Mass balance calculations have been performed in each run treating sunflower oil as tristearin and calculating the expected weight loss in each run taking into account the conversion and the total yields to hydrocarbons, free fatty acids, and esters. Considering that the reaction is not accompanied by density change and subtracting also the volume of the samples removed, we calculated the volume of the reaction mixture expected to remain in the reactor after each run. This volume differs less than ±3% to that measured at the end of each run.

Although the usual practice in this domain is to evaluate the catalysts at reactant volume (ml) to catalyst mass (g) ratio in the range 2–10 or at LHSV values for continuous reactors in the range 1–2 h^{-1} [13], we have decided to perform our evaluation at very high ratio of reactant volume to catalyst mass (100 ml/g) and reaction time of 9 h corresponding to LHSV equal to 11.1 h^{-1}. However, the most active catalyst was also evaluated at reactant volume to catalyst mass equal to 10 ml/g and reaction time of 5 h corresponding to LHSV equal to 2 h^{-1}, namely close to the conditions frequently reported in the literature [13]. Under the latter conditions we have also tested the most active catalyst for the SDO of WCO.

3. Results and discussion

3.1. Catalysts characterization

The catalysts synthesized together with their several textural characteristics are illustrated in Table 2.

The ex-situ SEM microphotographs recorded at various magnifications showed the presence of micro grains of different sizes and macro pores between the micro grains (Fig. SM1). In all cases the topo-elemental SEM–EDX analyses showed catalyst compositions very close to the nominal ones. Moreover, the SEM-EDX measurements performed at various points along the diameter of the cylindrical extrudates cross section indicated uniform profiles of Mo and Ni for all catalysts studied. Finally, the SEM-EDX measurements of the Mo and Ni concentrations performed in spent catalyst samples have shown that there is no measurable leaching of these metals upon catalytic reaction.

Fig. 1 illustrates the pore size distributions determined for the carrier and the fresh reduced supported catalysts.

A single peak distribution centered at about 8–9 nm is observed in all cases. This is in line with the relatively high specific surface areas and the small mean pore diameters determined for all samples (Table 2). The fact that the BET-SSA values obtained (Table 2) are very close to the BJH −SSA values (not presented) and the fact that the BJH-specific pore volume values (Table 2) are very close to those determined by dry impregnation with water (not presented) clearly indicates that the range 2–100 nm is sufficient to characterize the actual pore structure of the samples studied. The active phase loading (Ni + Mo) adopted in this work does not exceed the monolayer coverage of the alumina. Thus, a very good dispersion of the supported species (not detectable by XRD) is expected. This might explain why the prepared catalysts and the bare alumina exhibit similar pore size distributions. However, one may point out a decrease in the population of the pores with pore sizes 8–9 nm, more pronounced in the samples containing Mo (Fig. 1, left). It could be attributed to blocking of the mouths of a portion of the pores by the molybdenum nanoparticles formed. The effect is more intense in the sulphided samples (Fig. 1, right) in line with the decrease in the specific surface area and specific pore volume (entries 8 and 9 in Table 2).

The XRD patterns of the catalysts are illustrated in Fig. 2. The peaks at 2θ equal to 66.82, 45.83, 37.63, 39.52, and 60.51° reveal the presence of γ-alumina (JCPDS 29-0063) in all samples. The appearance of diffraction peaks at 26.0 and 53.3° reveals the formation of MoO_2 (JCPDS 32-0671) crystals in the sample with the maximum Mo content. This is also manifested by the important increase of ratio "intensity of the peak at 37.63° to that at 39.52°" due to the contribution of the second peak of MoO_2 at 36.9°. However, MoO_2 crystals are not detected in the samples containing less amounts of molybdenum. This could be attributed to that the decrease in the Mo loading is related to a change in the Mo-oxo species formed

Table 2
Symbols and several characteristics of the catalysts prepared (specific surface area (SSA), specific pore volume (PV) and mean pore diameter (MPD)).

Entry	Sample[a]	Ni/Mo% wt	$\frac{Ni}{Ni+Mo}$	SSA (m^2/g)	PV (cm^3/g)	MPD (nm)
1	Al_2O_3	–	0	260	0.66	6.6
2	4Ni	9.2	1	238	0.61	6.6
3	3.5Ni0.5Mo	8.0/2.0	0.87	205	0.54	6.7
4	3Ni1Mo	7.0/6.5	0.75	221	0.53	6.3
5	2Ni2Mo	5.0/12.0	0.50	212	0.50	6.3
6	1Ni3Mo	2.5/17.0	0.25	228	0.53	6.3
7	4Mo	24.0	0	199	0.46	6.3
8	1Ni3Mo-S	2.5/17.0	0.25	165	0.42	6.4
9	3.5Ni0.5Mo-S	8.0/2.0	0.87	152	0.41	6.3

[a] The first and the second number in the formulas indicate the nickel and Mo content, respectively, in atoms per nm^2 of the carrier. The samples in the entries 8 and 9 are sulphided ones.

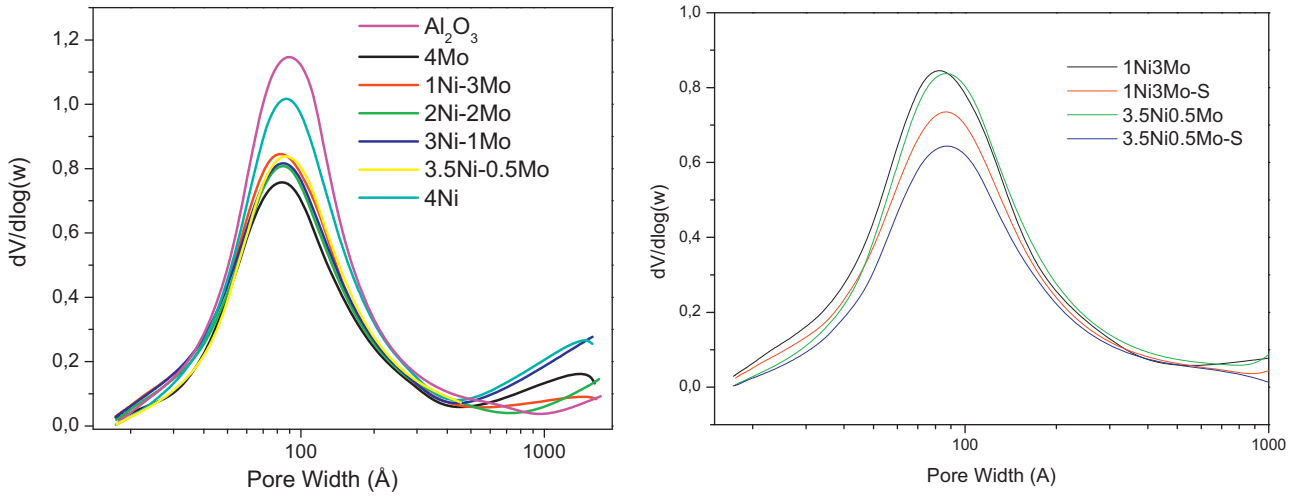

Fig. 1. Pore size distribution curves obtained for the fresh reduced catalysts studied. The symbols for the various samples are indicated.

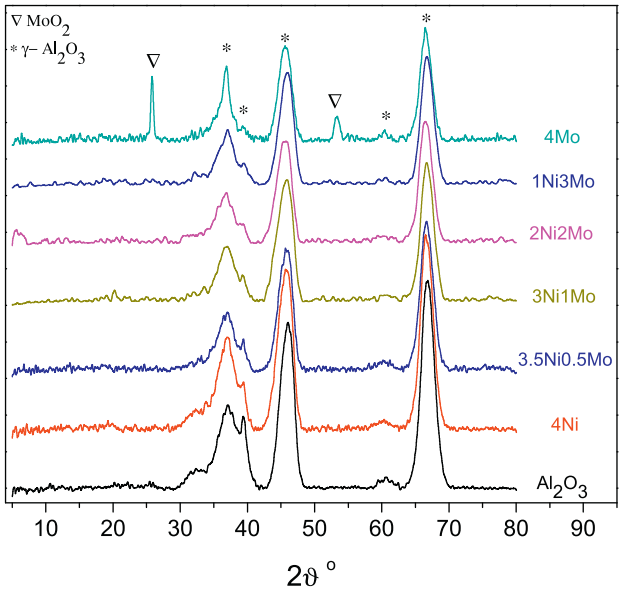

Fig. 2. The XRD patterns obtained for the fresh reduced catalysts studied.

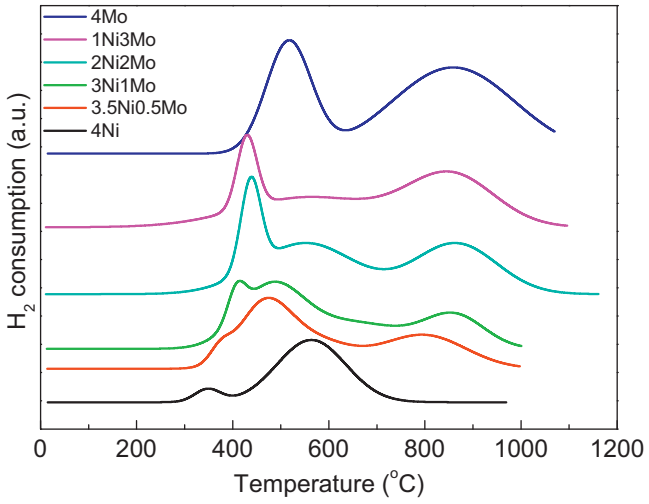

Fig. 3. Temperature programmed reduction profiles of the catalysts studied.

on the alumina surface. This point will be further investigated by the XPS together with additional supported phases not detected by XRD.

The reducibility of the supported phases and their interaction with the support were studied via TPR experiments. Fig. 3 illustrates the TPR profiles of the catalysts studied. The TPR curve of 4Mo sample exhibits two reduction peaks centered at 517 and 859 °C. The former is attributed to the reduction of Mo-oxo species from Mo^{6+} to Mo^{4+} [29,30], and the latter is assigned to the further reduction from Mo^{4+} to Mo^0 [31,32].

The TPR profile of monometallic Ni catalyst (4Ni) presents two reduction peaks centered at 347 and 563 °C. The first, minor, peak is assigned to the reduction of NiO loosely bonded on the support surface [33,34]. The small size of this peak shows that the relative amount of these species is very low. The second peak is assigned to the reduction of well dispersed NiO moderately interacted with support surface [35,36]. The absence of a peak at about

800 °C indicates no formation of significant quantities of $NiAl_2O_4$ [37].

Incorporation of Mo-oxo species in the Ni catalyst (3.5Ni0.5Mo) efficiently affects both the TPR profile and centered temperatures. More precisely, four peaks appear centered (after deconvolution) at 374, 464, 561, and 796 °C. The peak assigned to the NiO loosely bonded on the support surface is shifted at higher temperature (347 °C → 374 °C) revealing an increase of its interaction with the support or Mo-oxo species. The second peak attributed to NiO moderately interacted with support has shifted at lower temperature (563 °C → 464 °C) showing that the incorporation of Mo-oxo species facilitates the reduction of the well dispersed NiO. This is in accordance with the XPS results (see Table 4, column 6). The peak at 561 °C, first reduction step of Mo-oxo species ($Mo^{6+} \rightarrow Mo^{4+}$), is shifted 46 °C higher than the corresponding peak appeared in the TPR profile of 4Mo sample. This suggests stronger interactions of these species with the support surface. It is well known that low surface concentration of Mo-oxo species favors the formation of monomeric tetrahedral units strongly interacted with alumina surface while higher concentrations are related to the polymeric octahedral entities moderately interacted with the support surface [38]. Previous studies revealed that the reduction of octahedral Mo-oxo species is easier than that of tetrahedral ones [39,40]. The higher temperature peak ($Mo^{4+} \rightarrow Mo^0$) is shifted to lower temperature (859 °C → 796 °C) indicating an interaction between Ni and Mo phases [41].

The increase of the Mo content and the simultaneous decrease of Ni content have two main effects on the TPR profiles. The peaks corresponding to Mo-oxo species reduction approach those of the 4Mo sample. The two peaks assigned to NiO reduction are convoluted to one peak appearing at temperatures in between. This suggests the formation of only one NiO species in good interaction with Mo phase [30].

Fig. 4 displays detailed X-ray photoelectron spectroscopy (XPS) scans for the Mo3d core level spectrum of the fresh reduced samples studied. The peak is analyzed into two doublets with spin-orbit splitting 3.3 eV. The component with binding energy of $Mo3d_{5/2}$ at 232.3 ± 0.1 eV associated with Mo at the higher oxidation state (Mo^{6+}) whereas the component at about 230.5 eV is assigned to MoO_x, ($x < 3$) in which Mo is found at oxidation state $+4 \leq z \leq +5$ [42].

The XPS results, illustrated in Fig. 4, show the formation of both the MoO_3 and the reduced MoO_x phases. The first one is very well dispersed and thus it cannot be detected by XRD. The aforementioned statement that "the decrease in the Mo loading is related to change in the Mo-oxo species formed on the alumina surface" is corroborated by the XPS results. In fact, inspection of Fig. 4 and Table 3 (sixth column) clearly shows that the relative contribution of the MoO_x to the whole supported molybdenum increases with the Mo content.

Fig. 5 shows the deconvoluted $Ni2p_{3/2}$ peaks of the Ni containing fresh reduced samples. In order to analyze the Ni2p peak, reference samples (NiO, Ni foil and $NiAl_2O_4$) were also measured. The peak is deconvoluted into three chemical states. The peak at 852.8 ± 0.1 eV is assigned to Ni^0 chemical state. The component at 855.9 ± 0.1 eV is assigned to Ni^{2+} chemical state (NiO or NiOOH) and the component at 856.5 ± 0.1 eV to $NiAl_2O_4$ chemical state.

From the total peak area of $Ni2p_{3/2}$, Mo3d, O1s and Al2p photoelectrons and the relative sensitivity factors, the average atomic surface composition (% atoms) has been obtained. Moreover, from the peak area of the deconvoluted peaks corresponding to Ni^0, NiO, $NiAl_2O_4$ and Al2p we have calculated the ratios Ni^0/Al, NiO/Al, $NiAl_2O_4$/Al and (Ni^0 + NiO)/Al. The values of the above parameters were compiled in Table 3.

Inspection of Fig. 4 and Table 3 shows the formation of three nickel phases in all fresh reduced samples containing nickel, namely metallic nickel, nickel oxide and nickel aluminate. It seems that the experimental conditions adopted for the activation of the samples do not allow the complete reduction of NiO into Ni^0. Nevertheless, this is very probable under the very hard reaction conditions (very high hydrogen pressure and high reaction time). XPS analysis performed on two spent samples ($4Ni_{sp.}$ & $3.5Ni0.5Mo_{sp.}$, see Figs. S_2–S_4 and Table 3) confirms this statement. In fact, inspection of Table 3 shows that Ni^0/Al ratio increases in both the aforementioned spent samples. This clearly shows that in the un-promoted spent sample all the NiO is reduced into Ni^0 whereas the $NiAl_2O_4$ resists markedly to the reduction. The reduction of nickel oxide takes also place, but in lesser extent in the spent sample promoted by M◯ (most active sample). It seems that the presence of Mo oxides retards the nickel oxide reduction in agreement to the TPR results concerning the reduction of loosely bonded NiO. Moreover, we may observe the considerable increase of the $\%MoO_x$ due to the reduction of MoO_3.

The values obtained for the % atomic surface composition of Ni and Mo on the spent catalysts are very close to the corresponding ones determined on the fresh catalysts excluding considerable sintering during reaction. On the other hand, we have to mention that no increase of carbon content on the surface of the spent catalysts examined by XPS has been observed. This indicates that extensive coking does not take place on the catalysts surfaces during 9 h of reaction. From the above one can conclude that considerable deactivation does not take place upon reaction for 9 h.

In view of the above the nickel involved in both the Ni^0 and NiO phases is considered to catalyze the SDO of SO and WCO. This is the reason for which the values of (Ni^0 + NiO)/Al are also compiled in Table 3 (9th column). In contrast, the inactive nickel aluminate formed upon activation of the catalysts requires much higher temperature to be reduced than that of the reaction temperature [34]. We consider therefore that this phase is present in the catalyst under our reaction conditions.

Table 3 also shows a decrease in all nickel surface species formed on the support surface with the decrease in the nickel loading. This is rather expectable. However, it is remarkable that the addition of small amount of molybdenum (3.5Ni0.5Mo sample) brings about a selective decrease of the catalytically inactive $NiAl_2O_4$ [43] keeping the value of the (Ni^0 + NiO)/Al practically constant though the nickel content is decreased. It is probable that the well dispersed Mo-oxo species (Fig. 6), formed first on the support surface, decreases the nickel species-support interactions upon the second impregnation step and activation, inhibiting thus the formation of nickel aluminate.

In order to investigate the Mo and Ni dispersion in the samples studied, the %Mo and %Ni surface atoms taken from Table 3 were plotted against the nominal Mo and Ni surface densities, respectively. The plots are depicted in Fig. 6. The linear dependences of the %Mo and %Ni surface atoms determined by XPS on the corresponding Mo and Ni surface densities indicate constant, presumably very high, Mo and Ni dispersion on the whole range of the compositions.

Inspection of Fig. 6 indicates that the dispersion of molybdenum is better than that of nickel. Moreover, the calculation of the values of the $Ni/[Ni + Mo]_{XPS}$ atomic ratio from the data of Table 3 showed that these values are slightly smaller than the corresponding bulk values illustrated in Table 2, indicating again a better dispersion of molybdenum compared to that of nickel.

3.2. Catalysts evaluation

Evaluation of the prepared catalysts was performed in semi-batch reactor at 310 °C, 40 bar H_2 pressure, and 100 ml/min H_2 flow rate. Blank experiment performed under the same conditions revealed that SO does not undergo any transformation after 9 h.

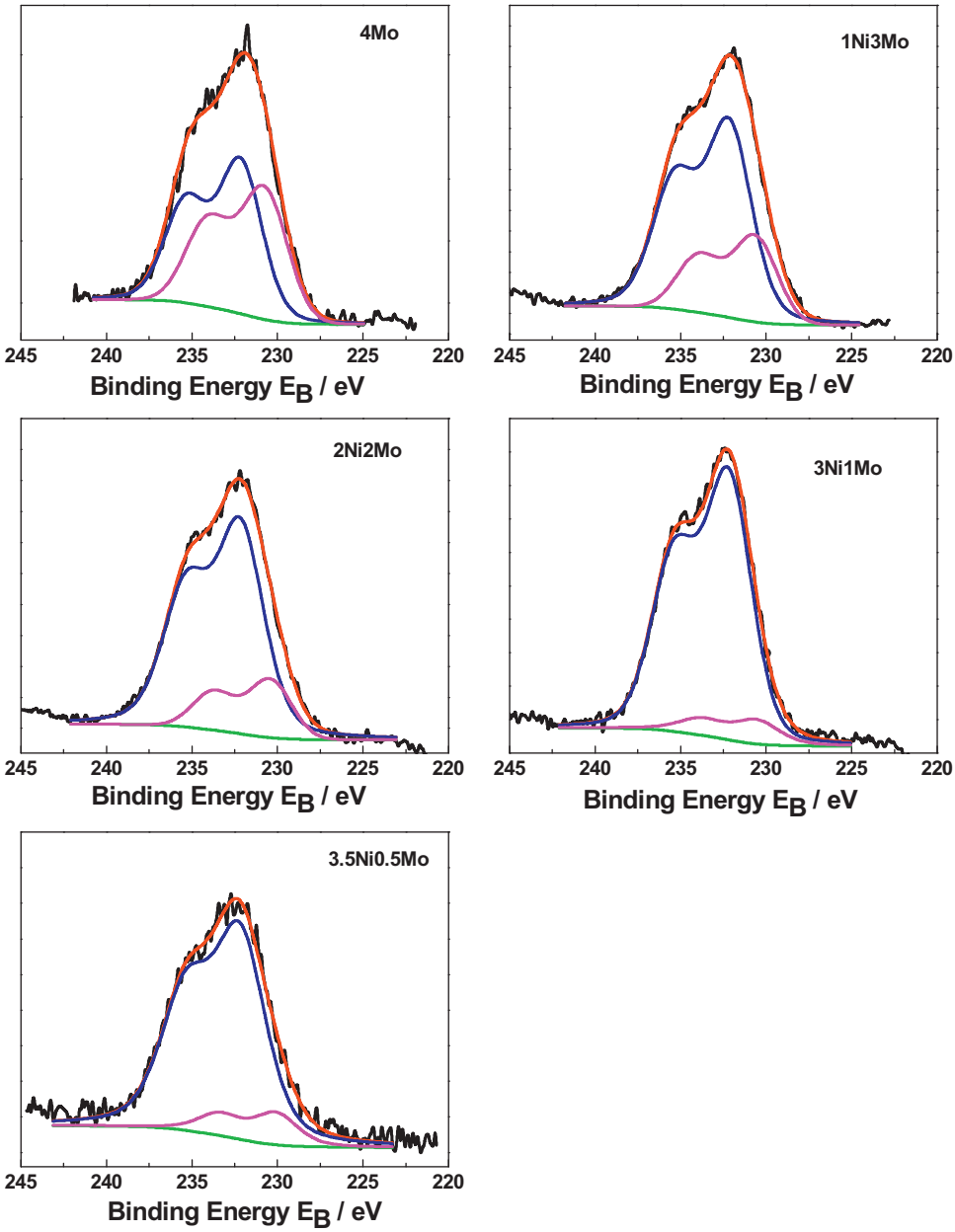

Fig. 4. XP spectra of the Mo3d core level of the Mo containing fresh reduced samples.

Table 3
Quantitative surface analysis of the fresh reduced and spent samples.

Sample	Surface atomic composition (atoms%)				%MoO_x	Ni^0/Al	NiO/Al	(Ni^0 + NiO)/Al	$NiAl_2O_4$/Al
	Ni	Al	O	Mo					
4Ni	3.3	27.8	68.9	–	–	0.021	0.074	0.095	0.023
$4Ni_{sp.}$	3.0	27.8	69.2	–	–	0.073	0.000	0.073	0.035
3.5Ni0.5Mo	2.83	26.9	69.2	1.04	11.9	0.039	0.051	0.090	0.016
$3.5Ni0.5Mo_{sp.}$	3.3	27.5	68.3	0.9	45.0	0.048	0.037	0.085	0.034
3Ni1Mo	2.48	29.9	66.1	1.52	10.7	0.012	0.055	0.067	0.016
2Ni2Mo	1.8	30.0	65.8	2.4	18.4	0.006	0.044	0.050	0.001
1Ni3Mo	0.93	30.0	66.2	2.8	28.2	0.002	0.027	0.029	0.001
4Mo	–	29.0	65.6	5.5	45.9	–	–	–	–

A representative chromatogram taken by sampling the liquid phase of the reactor in presence of the most active catalyst (3.5Ni0.5Mo) is illustrated in Fig. S_5. Normal alkanes in the diesel range (n-C17, n-C18, n-C15 and n-C16) have been detected in the liquid phase of the reactor but not remarkable amounts of alkanes with smaller number of carbon atoms (hydrocracking products). Intermediate compounds such as octadecanol, stearic acid, propyl and methyl esters, bigger esters and saturated diglycerides as well as un-reacted triglycerides have been also detected. The GC–MS spectra confirmed the chromatographic results. In the gas phase

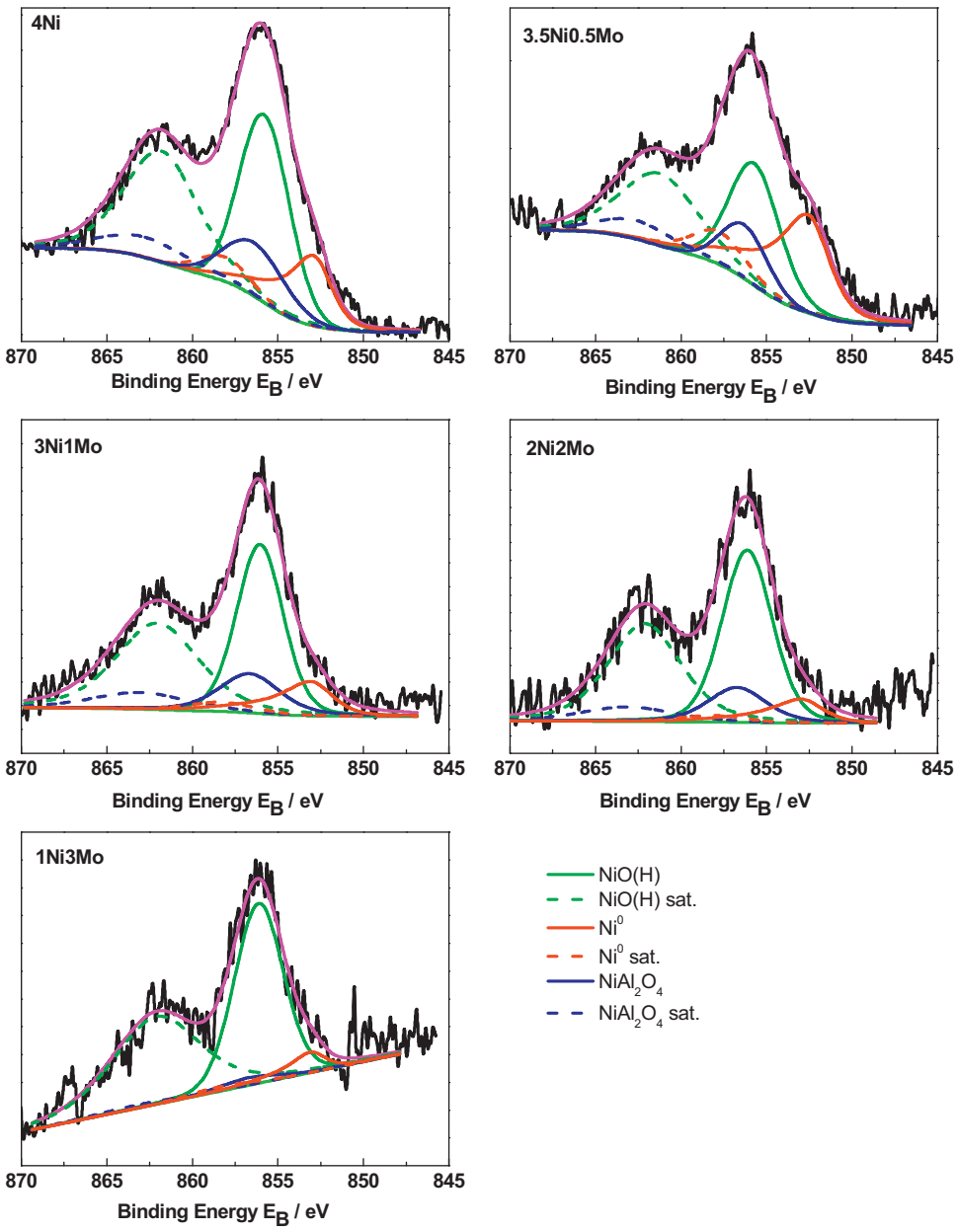

Fig. 5. Deconvoluted $Ni2p_{3/2}$ XP Spectra of several of the Ni containing fresh reduced samples. The dotted curves correspond to the satellite peaks.

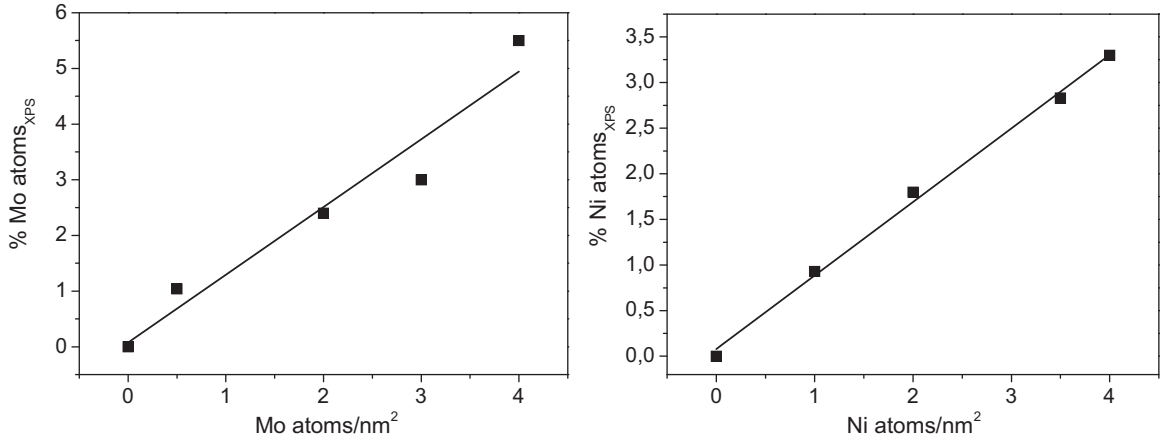

Fig. 6. The %Mo and %Ni surface atoms determined by XPS on fresh reduced catalysts versus the corresponding Mo and Ni surface densities.

Table 4
The sunflower oil conversions and yields of products obtained after 9 h of reaction time.

Entry	Sample	Conversion%	Yield to Esters wt%	Yield to Acids wt%	Yield to HC wt%	Yield to n-C15 wt%	Yield to n-C16 wt%	Yield to n-C17 wt%	Yield to n-C18 wt%
1	Al_2O_3	77	65[a]	9	–	–	–	–	–
2	4Ni	57	45	7.5	5	0.25	0.1	4.2	0.5
3	3.5Ni0.5Mo	81	45	11.5	14.2	0.4	0.3	8.0	5.5
4	3Ni1Mo	65	43	8.5	13.8	0.4	0.3	7.5	5.6
5	2Ni2Mo	74	56	9	9.2	0.25	0.3	4.2	4.5
6	1Ni3Mo	39	24	12	3	0.1	0.1	1.0	1.8
7	4Mo	47	36	11	0.3	0.02	0.01	0.1	0.17
8	1Ni3Mo-S	94	58	15	21	0.4	0.8	7.0	13
9	3.5Ni0.5Mo-S	91	71	12	7.3	0.2	0.2	4.0	2.9

[a] Polymer esters.

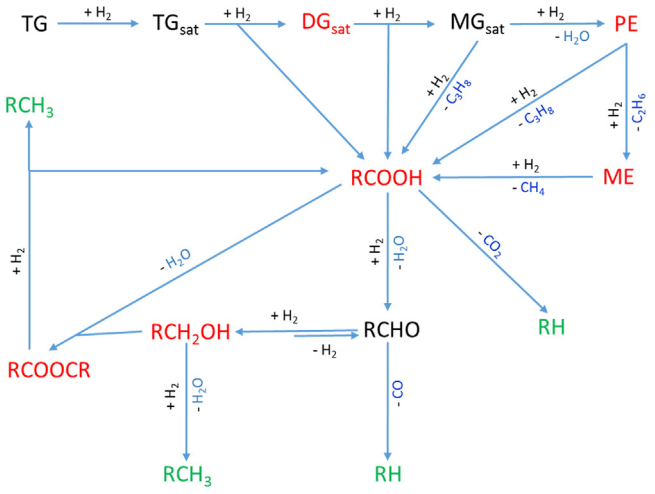

Fig. 7. Schematic representation of the SDO mechanism followed over Ni-Mo/Al_2O_3 reduced catalysts. Molecules written in green, red and blue are final, intermediate and gas phase products detected, respectively. (For interpretation of the references to colour in this figure legend, the reader is referred to the web version of this article.)

we have detected propane, ethane, CH_4, CO, and CO_2. The produced H_2O was condensed in an ice trap before on line gas phase analysis.

The liquid product derived over our catalysts, under conditions allowing the ranking of the catalysts studied, involves intermediate molecules, acids and esters. Therefore, this is not the final one. The final product will be derived over the most active catalyst under more suitable reaction conditions (e.g. lower reactant volume to catalyst mass ratio) and will be a mixture of n-$C_{17}H_{17}$, n-$C_{17}H_{18}$, n-$C_{17}H_{15}$ and n-$C_{17}H_{16}$ in which the heptadecane is the major product. This is very different for the composition of SO presented in the Section 2.1. Due to its composition the heat value of green diesel is very close to that of petrol diesel.

The detection of the above molecules is in accordance to the SDO mechanism proposed over the nickel based catalysts [13]. This can be schematized as follows (Fig. 7).

It can be seen that the first step of this scheme is the hydrogenation of the C=C bonds of the natural triglycerides. This is followed by the gradual hydrogenolysis of the O—C bonds in the side of glycerol backbone and the formation of free fatty acids, di-, mono-glycerides, propyl, ethyl and methyl esters of fatty acids as well as propane, ethane and methane. The fatty acids in the third step undergo reduction resulting to aldehydes and then to alcohols. These compounds are in equilibrium. The aldehydes are decarbonylated producing alkanes (n-C17 and n-C15) and CO whereas the alcohols are dehydrated and the intermediate olefins are hydrogenated resulting to alkanes (n-C18 and n-C16). In the same time the intermediate alcohols react with the intermediate fatty acids producing bigger esters. On the other hand, some of the free fatty acids undergo decarboxylation producing CO_2 and hydrocarbons with one carbon atom less than those of the corresponding initial acids.

The above mechanistic scheme (Fig. 7) indicates that the only end products in the liquid phase are the normal alkanes whereas the other products are intermediate ones which are in agreement to our kinetic results. Typical kinetic curves are illustrated in Fig. 8. In fact, we may observe that the conversion and the total yield in n-alkanes increase monotonically with the reaction time. In contrast, the total yield in the intermediate fatty acids or esters passes from a maximum or remain practically constant.

The values of the kinetic parameters obtained for the SDO of the sunflower oil at reaction time 9 h over the catalysts studied are compiled in Table 4.

We observe that the carrier exhibits considerable activity concerning the transformation of the triglycerides into fatty acids and esters (entry 1, columns 4 and 5). Almost all the esters produced are polymer esters. Thus, bare alumina does not catalyse any step of the aforementioned mechanistic scheme (Fig. 7), resulting mainly to polymerization products (poly-esters) and a small amount of free fatty acids. This explains the absence of hydrocarbons in the liquid phase after 9 h (entry 1, column 6). Concerning the % yield to hydrocarbons, which is the most important parameter from the practical point of view, the activity of nickel catalyst is greater than that of molybdenum catalyst (entries 2 and 7, column 6). Moreover, nickel (molybdenum) phases favour decarbonylation of intermediate aldehydes and decarboxylation of intermediate fatty acids (dehydration of intermediate alcohols) (Fig. 7, Table 4 entries 2–7, columns 7–10) in agreement to the literature [13].

The variation of the %yield to n-alkanes with the composition of the supported catalysts is illustrated in Table 4 (entries 1–7, column 6) and Fig. 9 (black curve). The promoting action of molybdenum is obvious. The yield takes its maximum value for a $\frac{Ni}{Ni+Mo}$ atomic ratio at about 0.8, very close to 0.87 corresponding to the most active sample, 3.5Ni0.5Mo (Table 4, entry 3, column 6).

This ratio is very different to the synergistic ratio, $\frac{Ni}{Ni+Mo} = 0.3$, concerning the conventional NiMo/γ-Al_2O_3 catalysts in their sulphided form used in the HDS of petroleum fractions [21]. The reduced catalyst 1Ni3Mo with a $\frac{Ni}{Ni+Mo}$ atomic ratio (0.25) approaching the latter ratio showed very low activity (Table 4, entry 6, column 6). In contrast, the sulphided sample, 1Ni3Mo-S, with the typical synergistic ratio for the HDS reactions showed also the maximum activity in the SDO of SO (Table 4, entry 8 and column 6), whereas the sulphided sample, 3.5Ni0.5Mo-S, showed much lower activity than its reduced counterpart (Table 4, entries 3 and 9, column 6). In conclusion, the critical synergistic ratio is similar for HDS and SDO for the NiMo/γ-Al_2O_3 catalysts in their sulphided form (about 0.3) but this ratio is very different for the SDO concerning the reduced form of the catalysts (about 0.8). A plausible explanation is that the active sites in the sulphided phase are located at MoS_2 slabs decorated by nickel ions (NiMoS phase) [21] whereas the active sites in the reduced state are metallic nickel atoms

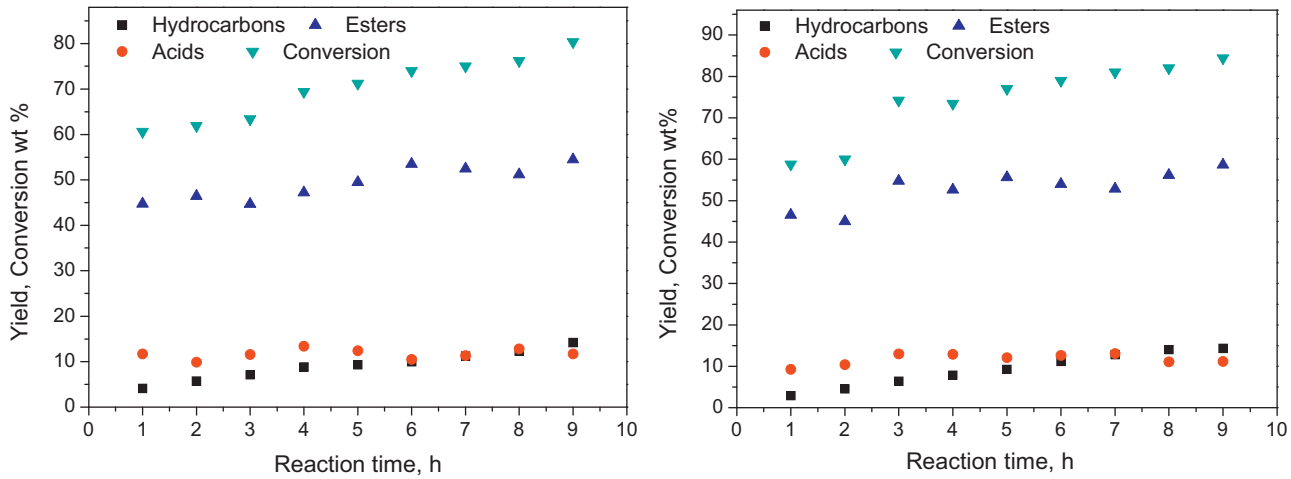

Fig. 8. Kinetic curves for the SDO of SO (left) and WCO (right) over the catalyst 3.5Ni0.5Mo.

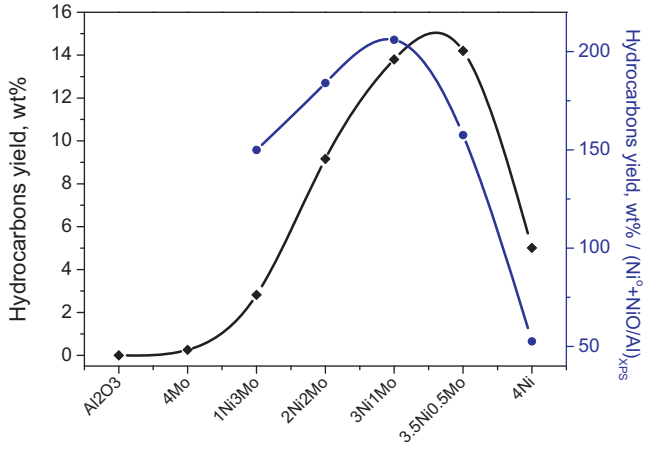

Fig. 9. Variation of the wt% yield to hydrocarbons (black curve) and the intrinsic activity expressed as wt% yield to hydrocarbons per $(Ni^0 + NiO)/Al]_{XPS}$ (blue curve) measured over the reduced catalysts. (For interpretation of the references to colour in this figure legend, the reader is referred to the web version of this article.)

promoted by MoO_3 or MoO_x (with Mo oxidation number between 5 and 4).

From the practical point of view the most important observation is that the simple change of the atomic $\frac{Ni}{Ni+Mo}$ ratio of the reduced NiMo/γ-Al_2O_3 catalysts from 0.25 to about 0.87 increases the percentage yield to normal alkanes in the diesel range by a factor of 14.3/3 = 4.77. The increase is actually impressive though the maximum yield obtained over the reduced NiMo/γ-Al_2O_3 catalyst remains lower than that obtained over the typical sulphided NiMo/γ-Al_2O_3 catalyst (Table 4, entries 3 and 8, column 6). The detection of the synergistic ratio for the NiMo/γ-Al_2O_3 reduced catalysts calls for additional research *concentrated on this ratio* for further improvement of the catalytic performance of these catalysts, mainly using suitable dopants [14–19].

The aforementioned $\frac{Ni}{Ni+Mo}$ synergistic ratio (about 0.8) concerns the *specific activity* which is the most important from the applications viewpoint. This value of the synergistic ratio may be considered as *apparent one* because it concerns the bulk composition of the catalysts. In order to probe the *true* synergistic ratio we have plotted the parameter "% yield to hydrocarbons/$[(Ni^0 + NiO)/Al]_{XPS}$" against the composition (Table 4, column 9 and Fig. 9, blue curve). As already mentioned (Section 3.1) NiO is transformed into metallic nickel under our very hard reaction conditions. This is not the case with the inactive $NiAl_2O_4$ which is reduced in much higher temperature [34]. Therefore, the parameter "% yield to hydrocarbons/$[(Ni^0 + NiO)/Al]_{XPS}$" expresses the intrinsic activity taking into account also the influence of the Mo phases on the formation of nickel aluminate. Fig. 9 (blue curve) shows that the Mo promotion is also manifested for the intrinsic activity. However, the true $\frac{Ni}{Ni+Mo}$ synergistic ratio is located at about 0.75 which correspond to the sample 3Ni1Mo. The small increase in the specific activity going from the sample 3Ni1MoAl to the sample 3.5Ni0.5Mo (Table 4, entries 3 and 4, column 6) is simply due to the increase in the nickel content.

Overall, the promotion of nickel by Mo oxides should be attributed to three actions of these oxides: (i) to the impressive decrease of the amount of the catalytically inactive surface nickel aluminate (Table 3) especially in the sample with the minimum Mo content (ii) to the increase of the surface concentration of the metallic Ni in the aforementioned most active sample (Table 3) and (iii) to the acceleration of the dehydration step of the intermediate alcohols (Fig. 7) evidenced by the yield of n-C18 with respect to n-C17 (Table 4).

As already mentioned in the experimental part, in order to facilitate the comparison of our results with those of the literature we have performed the evaluation of the most promising sample (3.5Ni0.5Mo) under the conditions described in the experimental part but for reactant volume to catalysts mass ratio equal to 10 ml/g. In this experiment we replaced the pure SO by a 10% v/v solution of SO in dodecane. Under the same conditions we have also tested the aforementioned catalyst for the SDO of WCO. A complete transformation of SO and WCO into various products was obtained after 5 h. This corresponds to an LHSV value equal to 2 h^{-1}, namely close to the conditions frequently reported in the literature [13].

The %yield for the various products is illustrated in Fig. 10. With the exception of very small amounts of octadecanol and negligible amounts of big esters, all the products obtained are normal alkanes in the diesel range. This concerns the SDO of SO and WCO. Therefore, another important finding of the present work is that one may obtain a complete transformation of SO and WCO using the catalyst 3.5Ni0.5Mo with $\frac{Ni}{Ni+Mo}$ ratio at about 0.87 and working at 310 °C, hydrogen pressure 40 bar, reactant volume to catalysts mass ratio equal to 10 ml/g and reaction time 5 h.

4. Conclusions

MoO_3/MoO_x (Mo oxidation number between 5 and 4) and Ni^0, NiO, $NiAl_2O_4$ phases are formed in the reduced monolayer NiMo/γ-Al_2O_3 catalysts prepared by successive incipient wetness

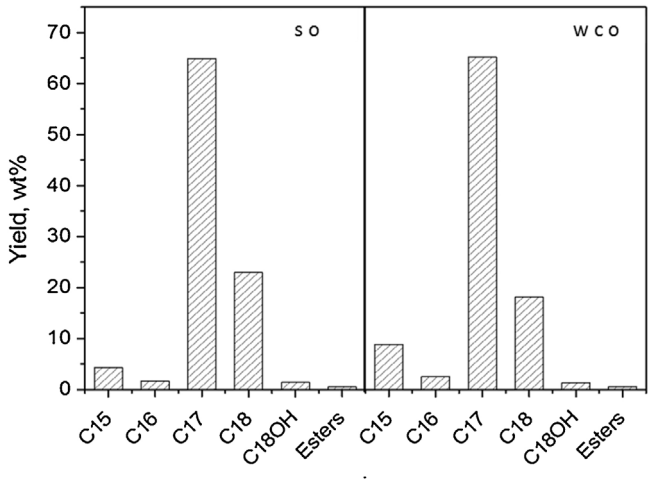

Fig. 10. Yields to various products obtained upon SDO of SO and WCO over the most active catalyst (3.5Ni0.5MoAl) under the experimental conditions described in the experimental part, using reactant volume to catalyst mass ratio equal to 10 ml/g and reaction time 5 h.

impregnation being very well dispersed on the support surface and uniformly distributed in the catalysts extrudates. These phases are mostly comprised from very small particles undetectable by XRD. Thus, the formation of the supported phases does not practically disturb the texture of the support. The composition of the catalysts somehow affects the relative amounts of the supported phases; the presence of Mo decreases drastically the amount of the inactive $NiAl_2O_4$, whereas the decrease in the Mo content causes a decrease in the MoO_3/MoO_x ratio.

The synergistic atomic ratio ($\frac{Ni}{Ni+Mo}$) in the NiMo/γ-Al_2O_3 r *educed* catalysts for the SDO of SO is located at about 0.8 and it is very different to that of the NiMo/γ-Al_2O_3 *sulphided* catalysts located at about 0.3 for both the HDS of petroleum fractions and the SDO of SO. A simple change of the atomic $\frac{Ni}{Ni+Mo}$ ratio in the NiMo/γ-Al_2O_3 *reduced* catalysts from 0.25 to 0.8 brought about an impressive increase of the% yield to hydrocarbons in the diesel range by a factor of 4.77.

A complete transformation of both SO and WCO into hydrocarbons in the diesel range (mainly heptadecane) was obtained over the most active catalyst at 310 °C, hydrogen pressure 40 bar, reactant volume to catalyst mass ratio equal to 10 ml/g and reaction time equal to 5 h. The latter two parameters correspond to a LHSV value (determined in the fixed bed reactors) equal to 2 h^{-1}.

Acknowledgment

Financial support of the present work from the "RESEARCH PROJECTS FOR EXCELLENCE IKY/SIEMENS" is gratefully acknowledged.

Appendix A. Supplementary data

Supplementary data associated with this article can be found, in the online version, at http://dx.doi.org/10.1016/j.apcatb.2017.02.045.

References

[1] N. Armaroli, V. Balzani, Angew. Chem. Int. Ed. 46 (2007) 52–66.
[2] J.M. Thomas, K.D.M. Harris, Energy Environ. Sci. 9 (2016) 687–708.
[3] R.C. Armstrong, C. Wolfram, K.P. De Jong, N.S. Gross, B. Boardman, A.J. Ragauskas, K. Ehrhardt-Martinez, G. Crabtree, M.V. Ramana, Nat. Energy 1 (2016), http://dx.doi.org/10.1038/NENERGY.2015.20, Art. Num. 15020.
[4] C. Zhao, T. Brück, J.A. Lercher, Green Chem. 15 (2013) 1720–1739.
[5] E.F. Aransiola, T.V. Ojuma, O.O. Oyekola, T.F. Madzimbamuto, D.I.O. Ikhu-Omoregbe, Biomass Bioenery 61 (2014) 276–297.
[6] S. Marx, Fuel Process. Technol. 151 (2016) 139–147.
[7] I. Kubickova, D. Kubicka, Waste Biomass Valorization 1 (2010) 293–308.
[8] R.W. Gosselink, S.A.W. Hollak, S.-W. Chang, J. van Haveren, K.P. de Jong, J.H. Bitter, D.S. van Es, ChemSusChem 6 (2013) 1576–1594.
[9] N. Taufiqurrahmi, S. Bhatia, Energy Environ. Sci. 4 (2011) 1087–1112.
[10] Y.K. Ong, S. Bhatia, Energy 35 (2010) 111–119.
[11] R.W. Gosselink, S.A.W. Hollak, S.-W. Chang, J. van Haveren, K.P. de Jong, J.H. Bitter, D.S. van Es, ChemSusChem 6 (2013) 1576–1594.
[12] A. Srifa, N. Viriya-empikul, S. Assabumrungrat, K. Faungnawakij, Catal. Sci. Technol. 5 (2015), 3693–3370.
[13] Ch. Kordulis, K. Bourikas, M. Gousi, E. Kordouli, A. Lycourghiotis, Appl. Catal. B Environ. 181 (2016) 156–196.
[14] J. Liu, C. Liu, G. Zhou, S. Shen, L. Rong, Green Chem. 14 (2012) 2499–2505.
[15] J. Liu, S. Yoda, J. He, L. Deng, K. Fan, L. Rong, Chem. Lett. 43 (2014) 310–312.
[16] J. Liu, K. Fan, W. Tian, C. Liu, L. Rong, Int. J. Hydrogen Energy 37 (2012) 17731–17737.
[17] C. Liu, J. Liu, G. Zhou, W. Tian, L. Rong, J. Taiwan Inst. Chem. Eng. 44 (2013) 221–227.
[18] C. Liu, J. Liu, G. Zhou, W. Tian, L. Rong, Environ. Prog. Sustain. 32 (2013) 1240–1246.
[19] K. Fan, J. Liu, X. Yang, L. Rong, Int. J. Hydrogen Energy 39 (2014) 3690–3697.
[20] H. Topsoe, B.S. Clausen, F.E. Massoth, Hydrotreating Catalysis—Science and Technology, Springer, Berlin, 1996.
[21] A. Al-Sharafi, A.Z. Sahin, T. Ayar, B.S. Yilbas, Renew. Sustain. Energy Rev. 69 (2017) 33–49.
[22] P.B. Weisz, W.O. Haag, P.G. Rodewald, Science 206 (1979) 57–58.
[23] G. Knothe, Prog. Energy Combust. Sci. 36 (2010) 364–373.
[24] S.B. Glisic, J.M. Pajnik, A.M. Orlovic, Appl. Energy 170 (2016) 176–185.
[25] X. Zhao, L. Wei, S. Cheng, J. Julson, G. Anderson, K. Muthukumarappan, C. Qiu, J. Renew. Sustain. Energy 8 (2016) 013109, http://dx.doi.org/10.1063/1.4941911.
[26] A.B. Chhetri, K. Chris Watts, M. Rafiqul Islam, Energies 1 (2008) 3–18.
[27] N. Spanos, H.K. Matralis, C. Kordulis, A. Lycourghiotis, J. Catal. 136 (1992) 432–445.
[28] B. Peng, X. Yuan, C. Zhao, J.A. Lercher, J. Am. Chem. Soc. 134 (2012) 9400–9405.
[29] H. Liu, C. Liu, C. Yin, Y. Chai, Y. Li, D. Liu, B. Liu, X. Li, Y. Wang, X. Li, Appl. Catal. B Environ. 174–175 (2015) 264–276.
[30] H. Liu, Y. Li, C. Yin, Y. Wu, Y. Chai, D. Dong, X. Li, C. Liu, Appl. Catal. B Environ. 198 (2016) 493–507.
[31] K. Soni, B.S. Rana, A.K. Sinha, A. Bhaumik, M. Nandi, M. Kumar, G.M. Dhar, Appl. Catal. B Environ. 90 (2009) 55–63.
[32] J. Zhang, Z. Xin, X. Meng, Y. Lv, M. Tao, Fuel 116 (2014) 25–33.
[33] Q. Liu, J. Gao, F. Gu, X. Lu, Y. Liu, H. Li, Z. Zhong, B. Liu, G. Xu, F. Su, J. Catal. 326 (2015) 127–138.
[34] A. Tribalis, G.D. Panagiotou, K. Bourikas, L. Sygellou, S. Kennou, S. Ladas, A. Lycourghiotis, C. Kordulis, Catalysts 6 (11) (2016), http://dx.doi.org/10.3390/catal6010011.
[35] S. Damyanova, B. Pawelec, K. Arishtirova, J.L.G. Fierro, Int. J. Hydrogen Energy 37 (2012) 15966–15975.
[36] E. Kraleva, M.-M. Pohl, A. Jurgensen, H. Ehrich, Appl. Catal. B 179 (2015) 509–520.
[37] M. Zaungouei, A.Z. Moghaddam, M. Arasteh, Chem. Eng. Res. Bull. 14 (2010) 97–102.
[38] K. Bourikas, C. Kordulis, A. Lycourghiotis, Catal. Rev. Sci. Eng. 48 (2006) 363–444.
[39] R. Nava, R.A. Ortega, G. Alonso, C. Ornelas, B. Pawelec, J.L.G. Fierro, Catal. Today 127 (2007) 70–84.
[40] S. Garg, K. Soni, T. Ajeeth Prabhu, K.S. Rama Rao, G. Murali Dhar, Catal. Today 261 (2016) 128–136.
[41] A. Wang, Y. Wang, T. Kabe, Y. Chen, A. Ishihara, W. Qian, P. Yao, J. Catal. 210 (2002) 319–327.
[42] M. Vasilopoulou, A.M. Douvas, D.G. Georgiadou, L.C. Palilis, S. Kennou, L. Sygellou, A. Soultati, P. Argitis, J. Am. Chem. Soc. 134 (39) (2012) 16178–16187.
[43] P.G. Savva, K. Goundani, J. Vakros, K. Bourikas, C. Fountzoula, D. Vattis, A. Lycourghiotis, C. Kordulis, Appl. Catal. B Environ. 79 (2008) 199–207.